PHYSICAL REVIEW C

NUCLEAR PHYSICS

THIRD SERIES, VOLUME 32, NUMBER 2 AUGUST 1985

Energy average of the scattering matrix in picket-fence models

C. H. Johnson
Oak Ridge National Laboratory, Oak Ridge, Tennessee 37831

C. Mahaux
Institut de Physique, Université de Liège, 4000 Liège, Belgium

R. R. Winters
Denison University, Granville, Ohio 43023

(Received 29 January 1985)

The optical-model potential at low energy is defined by the requirement that it yields a suitably defined energy average of the scattering function. It is argued that the quantities which appear in the expression for this energy average derived by Lane and Thomas in the framework of R-matrix theory can be identified with those which appear in a convenient parametrization of the fine structure cross section. The accuracy of this identification is illustrated with the help of various picket-fence models. We discuss the independence of the results with respect to the size of the energy domain covered by the experimental data and to the nature of the R-matrix boundary parameters. Also we discuss terms that can be included if one wishes to discuss fluctuations about a smooth average.

I. INTRODUCTION

Neutron elastic scattering cross sections exhibit narrow resonances for bombarding energies smaller than a few MeV. From an analysis of these cross sections one can determine the contribution of individual partial waves. This yields information on the average neutron-nucleus potential at low energy and in a specific angular momentum subspace, provided that one can relate this potential to the measured fine structure cross section. The latter problem was discussed many years ago[1–3] and, because of the availability of accurate measurements which extend up to a few MeV, has recently received renewed attention, see, e.g., Refs. 4–15.

The main purpose of the present paper is to show that one can easily and accurately determine the optical-model scattering function from the analysis of the resonance cross section, provided that one defines the average neutron-nucleus potential in such a way that it is a smooth function of energy. The latter property is in keeping with the definition adopted by most authors, who consider that possible dynamical structure effects should be treated explicitly, e.g., via the use of a coupled-channel analysis.

The existence of a simple algebraic relationship between the average scattering function and a convenient parametrization of the fine structure cross section is introduced in Sec. II and its accuracy is demonstrated in Sec. III. That discussion is carried out in the framework of picket fence models which allow us, using numerical integration, to determine accurately a smooth average scattering function and thereby to make detailed tests of our algebraic prescription. In Sec. IV we discuss experimental fluctuations from the idealized picket fence models. In Sec. V we show the relation to the optical model scattering function and in Sec. VI we discuss the insensitivity to the assumed boundary conditions. Section VII is our summary.

II. THE AVERAGE SCATTERING MATRIX

Let us for the sake of notational simplicity consider the case of s-wave elastic neutron scattering by a spin zero target. The R-matrix formulation of the scattering function reads

$$S(E)=e^{-2ika}\frac{1+ikaR(E)}{1-ikaR(E)}\ , \tag{2.1}$$

where $-ka$ in the exponential is the hard sphere scattering phase shift ϕ_0, the coefficient ka is the penetrability P_0, and the R function is given by

$$R(E)=\sum_{\mu}\frac{\gamma_\mu^2}{E_\mu-E}\ . \tag{2.2}$$

The γ_μ^2 and E_μ are the reduced width and energy of the

level μ, and the summation runs over all levels.

Lane and Thomas[1] have derived an algebraic expression for the energy average of $S(E)$ under the following main conditions:

(a) The quantity ka is not averaged over; this is discussed in Sec. V.

(b) The strength function is a smooth function of energy. The strength function $s(E)$ is defined by

$$s(E)=\langle\gamma_\mu^2\rangle/d \ , \tag{2.3}$$

where $\langle\gamma_\mu^2\rangle$ and d are average values of γ_μ^2 and of $(E_{\mu+1}-E_\mu)$ in an interval of size I centered on E. This condition will be fulfilled if one can choose the averaging interval I in such a way that

$$d \ll I \ll s(E)/\left|\frac{ds}{dE}\right| \ . \tag{2.4}$$

If these conditions are fulfilled, the average $\langle S(E)\rangle_I$ of $S(E)$ is given by[1]

$$\langle S(E)\rangle_I = e^{-2ika}\frac{1+ikaR(E+iI)}{1-ikaR(E+iI)} \ , \tag{2.5}$$

with

$$R(E+iI)=\int_{-\infty}^{\infty}\frac{s(E')}{E'-E-iI}dE' \ . \tag{2.6}$$

One has[1]

$$R(E+iI)\simeq\bar{R}(E)+i\pi s(E) \ , \tag{2.7}$$

where

$$\bar{R}(E)=\mathrm{P}\int_{-\infty}^{\infty}\frac{s(E')}{E'-E}dE' \ . \tag{2.8}$$

Here, P denotes the principal value integral.

As pointed out in Ref. 11 the problem encountered when trying to apply Eqs. (2.5)–(2.7) is that $s(E)$ is only known for energies between a lower energy E_l to an upper energy E_u covered by the experimental data. We shall denote this "experimental domain" by the letter D. We now describe how $\langle S(E)\rangle_I$ can nevertheless be determined from the analysis of the experimental data. Let us write

$$S(E)=e^{-2ika}\frac{1+ika\,[R^{\mathrm{ext}}(E)+R^{\mathrm{int}}(E)]}{1-ika\,[R^{\mathrm{ext}}(E)+R^{\mathrm{int}}(E)]} \ , \tag{2.9}$$

where

$$R^{\mathrm{int}}(E)=\sum_{E_\lambda\in D}\frac{\gamma_\lambda^2}{E_\lambda-E} \ , \tag{2.10}$$

$$R^{\mathrm{ext}}(E)=\sum_{\alpha\neq\lambda}\frac{\gamma_\alpha^2}{E_\alpha-E} \ . \tag{2.11}$$

The data determine $S(E)$ and related quantities in the experimental region D only; they do not yield the values of γ_α^2 and E_α. However, one can use the property that the strength function is smooth and write for *E contained inside D*

$$R^{\mathrm{ext}}(E)\approx\int_{-\infty}^{E_l}\frac{s(E')}{E'-E}dE'+\int_{E_u}^{\infty}\frac{s(E')}{E'-E}dE' \ . \tag{2.12}$$

Equation (2.8) shows that

$$R^{\mathrm{ext}}(E)\approx\bar{R}(E)-\mathrm{P}\int_{E_l}^{E_u}\frac{s(E')}{E'-E}dE' \ . \tag{2.13}$$

One can calculate $\langle S(E)\rangle_I$ from Eqs. (2.5) and (2.7) by identifying $\bar{R}(E)$ and $s(E)$ with the quantities $\tilde{R}(E)$ and $\tilde{s}(E)$ determined by parametrizing the experimental data with the following expressions:

$$S_p(E)=e^{-2ika}\frac{1+ikaR_p(E)}{1-ikaR_p(E)} \ , \tag{2.14}$$

where

$$R_p(E)=R_p^{\mathrm{ext}}(E)+\sum_{E_\lambda\in D}\frac{\gamma_\lambda^2}{E_\lambda-E} \ , \tag{2.15}$$

with

$$R_p^{\mathrm{ext}}(E)=\tilde{R}(E)-\mathrm{P}\int_{E_l}^{E_u}\frac{\tilde{s}(E')dE'}{E'-E} \ . \tag{2.16}$$

The strength function $\tilde{s}(E)$ is that observed in the domain D, and $\tilde{R}(E)$ is a simple parametric function which makes $R_p^{\mathrm{ext}}(E)$ a good approximation to $R^{\mathrm{ext}}(E)$. The subscript p denotes "parametrization." The logarithmic singularities of $R_p^{\mathrm{ext}}(E)$ at the extremities E_l and E_u of the domain approximately account for the property that the energy derivative of $R^{\mathrm{ext}}(E)$ increases near E_l and E_u because of the energy dependence of the tails of the resonances associated with poles E_α which lie outside of, but close to, the experimental domain. The accuracy of this approximation is demonstrated in Sec. III E.

III. PICKET FENCE MODELS

A. Definitions

Since the hard-sphere phase shift and the penetrability are kept fixed in the averaging process (see Sec. V), we may set $ka=1$ and consider the following model for values of E contained in the experimental domain $D=(E_l,E_u)$:

$$S(E)=\frac{1+iR_p(E)}{1-iR_p(E)} \ . \tag{3.1}$$

The following picket-fence models are characterized by the property that the poles E_λ are equidistant

$$E_{\lambda+1}-E_\lambda=d \ , \quad 1\leq\lambda\leq N \ , \tag{3.2a}$$

$$E_1=E_l+d/2 \ , \quad E_N=E_u-d/2 \ , \tag{3.2b}$$

and that the strength function $\tilde{s}(E)$ is either a constant (Sec. III C) or an increasing function of energy (Sec. III D). For each model we assume 20 levels in the experimental domain,

$$N=20 \ , \tag{3.3a}$$

$$E_l=0 \ , \quad E_u=1 \text{ MeV}. \tag{3.3b}$$

Finally we must parametrize $\tilde{R}(E)$ in order to fully specify the experimental cross sections. Specific values of $\tilde{R}(E)$, $\tilde{s}(E)$, and γ_λ^2 are given in the following sections for each model.

B. Numerical average

In order to check the accuracy of the algebraic prescription

$$\langle S(E)\rangle = \frac{1+i[\tilde{R}(E)+i\pi\tilde{s}(E)]}{1-i[\tilde{R}(E)+i\pi\tilde{s}(E)]} , \tag{3.4}$$

we shall compare it with a numerical average of the quantity $S(E)$ defined by Eqs. (3.1), (2.15), and (2.16). This numerical average is computed from the following formulas:[6]

$$\bar{S}(\bar{E}) = \int_{E_l}^{E_u} F_I(E,E')S(E')dE' , \tag{3.5}$$

where

$$\bar{E} = \int_{E_l}^{E_u} F_I(E,E')E'dE' \tag{3.6}$$

and

$$1 = \int_{E_l}^{E_u} F_I(E,E')dE' . \tag{3.7}$$

Here $F_I(E,E')$ is a weighting function centered on $E'=E$ whose width $2I$ is identified with the size of the averaging interval. Unless otherwise specified, we shall take the Lorentzian shape

$$F_I^L(E,E') = \frac{f_L(E)}{(E-E')^2+I^2} , \tag{3.8}$$

where $f_L(E)$ is determined by the normalizing condition (3.7). We emphasize, however, that the precise shape of the weighting function does not matter. We shall illustrate this property by also using the box weighting function

$$F_I^B(E,E') = f_B\theta(I-|E-E'|) . \tag{3.9}$$

The average of $S(E)$ cannot be uniquely defined for E close to E_l or E_u. Hence, we shall calculate the quantity $\bar{S}(\bar{E})$ only in the domain of E which corresponds to the energy interval

$$E_l+I<E<E_u-I . \tag{3.10}$$

Note that in this interval one has $\bar{E}=E$ in the case of the box average (3.9).

The quantity $\bar{S}(\bar{E})$ is complex. It can be represented by plotting the quantities $\bar{R}(\bar{E})$ and $\bar{s}(\bar{E})$ defined by the relation

$$\bar{S}(\bar{E}) = \frac{1+i[\bar{R}(\bar{E})+i\pi\bar{s}(\bar{E})]}{1-i[\bar{R}(\bar{E})+i\pi\bar{s}(\bar{E})]} . \tag{3.11}$$

This notation is in keeping with the one used in Sec. II. It is important to note that this expression in terms of a complex R function uses the same constant ϕ_0 and P_0 as used in the averaging process. Other representations of $\bar{S}(\bar{E})$ are also of interest;[6] we use one of those in Sec. VI.

We note that when averaging numerically the particular parametrization chosen to represent the function $R^{\text{ext}}(E)$ is irrelevant. All parametrizations which yield approximately the same $R_p^{\text{ext}}(E)$ for $E\in D$ will yield approximately the same average of $\bar{S}(\bar{E})$. We have checked this numerically for several parametrizations.

C. Constant strength function

We first investigate the case when all the widths γ_λ^2 are equal, i.e., when $\tilde{s}(E)$ is independent of energy. For the purpose of illustration, we choose

$$\gamma_\lambda^2 = 5 \text{ keV}, \tag{3.12}$$

whence

$$\tilde{s}(E) = 0.1 . \tag{3.13}$$

For this model and with the boundary radius $a=5.5$ fm, for example, we find the conventional strength function $\bar{\Gamma}_n^0/d$ to be 2.4×10^{-4}; this is a typical value for nuclei near $A=60$. Figure 1(a) shows the picket fence of γ_λ^2 and Fig. 1(b) shows the corresponding $\tilde{s}(E)$. For $\tilde{R}(E)$ we assume a linear function,

$$\tilde{R}(E) = 0.1+0.2E . \tag{3.14}$$

Linear functions with similar parameters have been used previously for actual data.[4,15] In Fig. 1(c) the dashed line shows $\tilde{R}(E)$ and the solid curve shows the $R_p^{\text{ext}}(E)$ calculated from Eq. (2.16).

We performed the numerical average of $S(E)$ using a Lorentzian weighting function with $I=100$ and 300 keV and also using box weighting with $I=200$ keV. In Fig. 2 the solid curves show the resulting average in form (3.11),

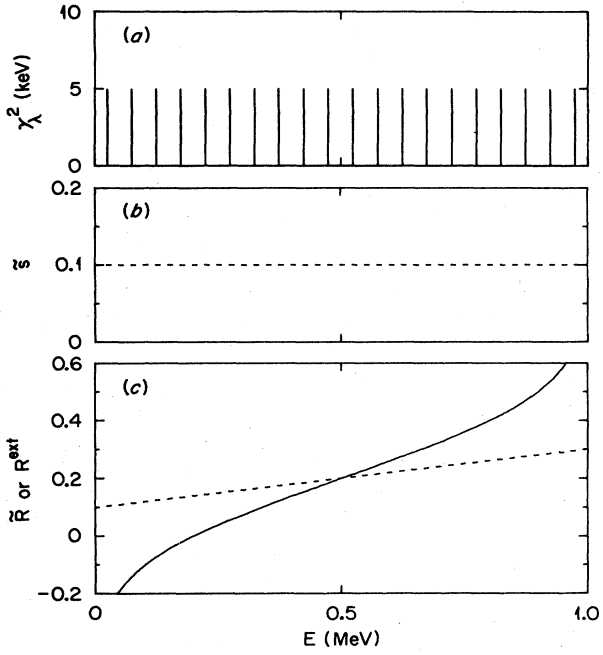

FIG. 1. Uniform picket fence model: (a) equally spaced levels of uniform reduced widths, (b) the strength function, (c) the external R function (solid) and $\tilde{R}$ (dashed).

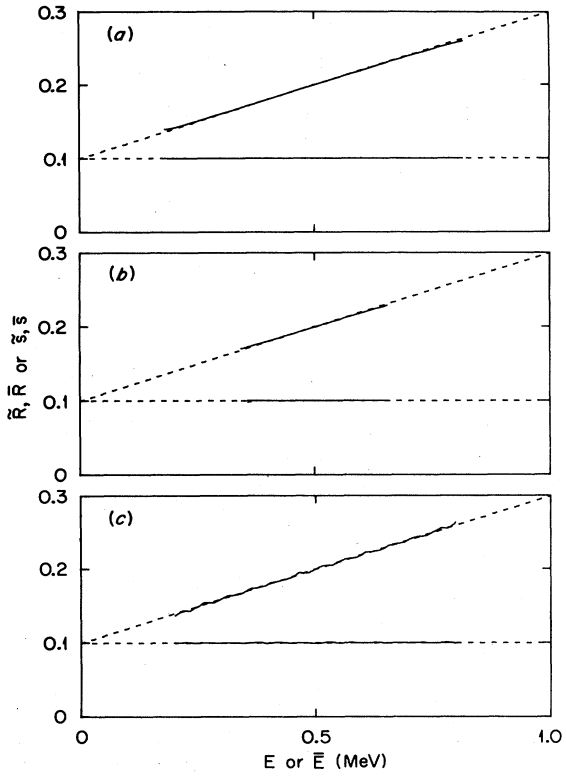

FIG. 2. Numerical averages of the uniform picket fence model: (a) average for Lorentzian weighting with $I=100$ keV, (b) Lorentzian weighting with $I=300$ keV, and (c) box weighting with $I=200$ keV. In each case the quantities $\bar{s}(\bar{E})$ and $\bar{R}(\bar{E})$ are shown, respectively, by horizontal and sloping solid curves for E between E_l+I and E_u-I. Dashed curves show $\tilde{s}(E)$ and $\tilde{R}(E)$ reproduced from Figs. 1(b) and (c).

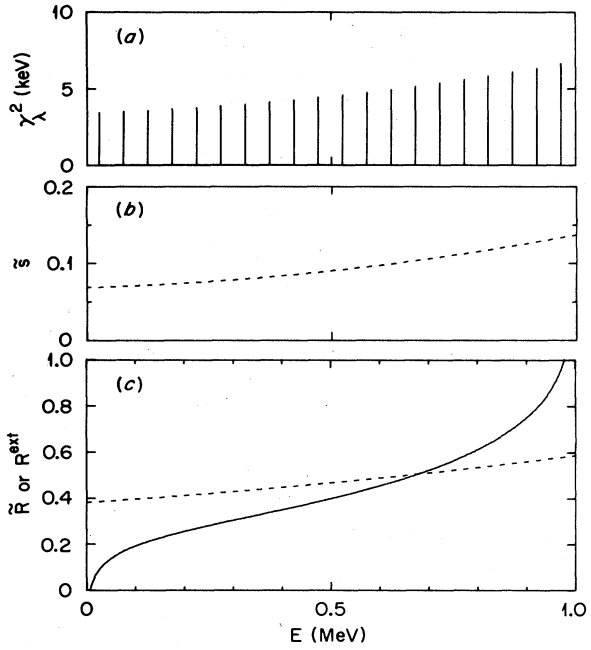

FIG. 3. Rising picket fence model: (a) reduced widths, (b) the strength function, (c) the external R function (solid) and $\tilde{R}$ (dashed).

i.e., as $\bar{R}(\bar{E})$ and $\bar{s}(\bar{E})$. The good agreement between these various averages confirms that the average of $S(E)$ is well defined and is practically independent of the shape of the weighting function and of the value of the averaging interval. Henceforth, we shall always use the Lorentzian weighting factor with $I=100$ keV ($=2d$).

The dashed lines in Fig. 2 show $\tilde{R}(E)$ and $\tilde{s}$ reproduced from Fig. 1. The good agreement between $\bar{R}(\bar{E})$ and $\tilde{R}(E)$ for $\bar{E}=E$ and between $\bar{s}$ and $\tilde{s}$ demonstrates the accuracy of the algebraic approximation (3.4) for the average of the scattering function. In this model with constant $\tilde{s}$ the approximation (3.4) coincides with the one proposed in Ref. 6.

D. Energy-dependent strength function

We now consider an example for which $\tilde{s}(E)$ is an increasing function of energy. For simplicity we could assume a linear function; however, we consider a quadratic form in order that our example can be used in Sec. VI to demonstrate the invariance of $\bar{S}(\bar{E})$ relative to boundary conditions for s-wave neutrons. If the picket fence model of Fig. 1 is assumed for s waves then the transformation to a larger boundary radius, as discussed in Sec. VI, yields $\tilde{s}$ and $\tilde{R}$ which are well described as quadratic in energy. For the strength function we have

$$\tilde{s}(E)=0.069+0.018E+0.05E^2\ , \tag{3.15}$$

where E is in MeV. This function is plotted in Fig. 3(b) and the corresponding γ_λ^2 are shown in Fig. 3(a). The E_λ are slightly less than the corresponding E_λ of Fig. 1(a) and have $d\simeq 49.8$ keV. (These slight variations are necessary for the example in Sec. VI.) The $\tilde{R}(E)$ is also quadratic,

$$\tilde{R}(E)=0.38+0.14E+0.07E^2\ , \tag{3.16}$$

and is shown by the dashed curve in Fig. 3(c). The solid curve shows $R_p^{\rm ext}(E)$ from Eq. (2.16). The difference in the shape of $R_p^{\rm ext}(E)$ relative to Fig. 1(c) results primarily because $\tilde{s}(E)$ is an increasing function of energy.

In Fig. 4, we compare $\tilde{R}(E)$ and $\tilde{s}(E)$ with the quantities $\bar{R}(\bar{E})$ and $\bar{s}(\bar{E})$ defined by Eq. (3.11), where $\bar{S}(\bar{E})$ is calculated numerically with the Lorentzian weighting function with $I=100$ keV. The good agreement between $\bar{R}(\bar{E})$ and $\tilde{R}(E)$ and between $\bar{s}(\bar{E})$ and $\tilde{s}(E)$ for $\bar{E}=E$ confirms the accuracy of the prescription (3.4).

We note that this prescription differs from the one which had been proposed in Ref. 6. The latter is inaccurate when the energy dependence of $\tilde{s}(E)$ is not negligible. The reason of this inaccuracy is reflected in the fact that the right-hand side of Eq. (3.28) of Ref. 6 is not a smooth function of E' as had been assumed there. Indeed, for E' close to E_u this quantity has a logarithmic singularity equal to $[\tilde{s}(E)-\tilde{s}(E_u)]\ln(E_u-E')$.

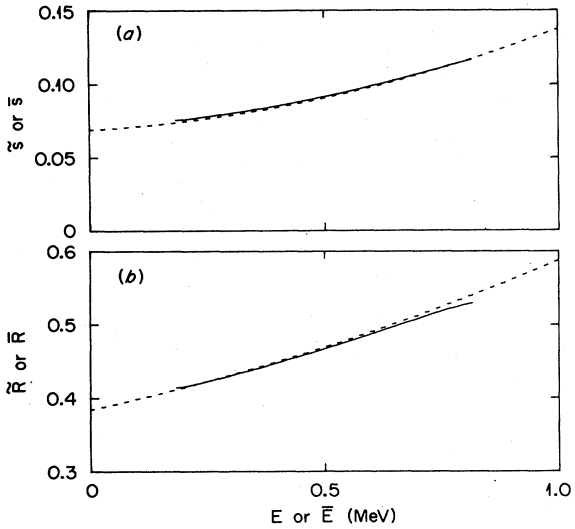

FIG. 4. Numerical average of the rising picket fence model for Lorentzian weighting with $I=100$ keV. Solid curves show the average quantities $\bar{s}(\bar{E})$ and $\bar{R}(\bar{E})$ plotted from E_l+I to E_u-I. Dashed curves show $\tilde{s}(E)$ and $\tilde{R}(E)$ reproduced from Figs. 3(b) and (c).

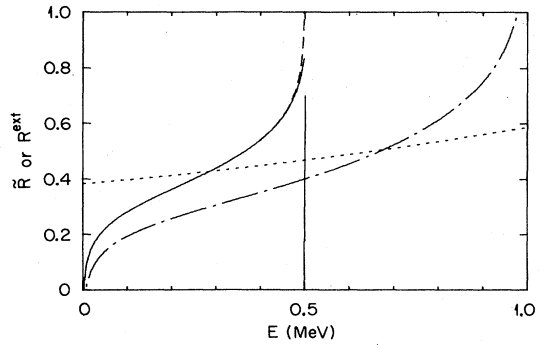

FIG. 5. A comparison of R external for two experimental domains. For the full domain the short-dashed and long-short dashed curves show, respectively, the $\tilde{R}$ and R^{ext} from Fig. 3(c). For the lower half domain, the solid and long-dashed curves show R^{ext} calculated, respectively, from discrete and continuous distributions in the upper half domain.

E. Dependence upon the size of the experimental domain

In the present section we illustrate the accuracy of the replacement in Eqs. (2.12) and (2.13) of the contribution of the external poles $\alpha\neq\lambda$ by a continuous distribution. By the same token, we demonstrate the innocuous character of the logarithmic singularities which appear in the parametrization (2.16) at the end points E_l and E_u of the experimental domain.

Let us consider the example discussed in Sec. III D, i.e., 20 resonances with a rising strength function in the interval $D_1=(E_l,E_{u1})$ with $E_l=0$ and $E_{u1}=1$ MeV. The corresponding value of the external R function is given by Eq. (2.16), namely

$$R_1^{\text{ext}}(E)=\tilde{R}(E)=\mathrm{P}\int_{E_l}^{E_{u1}}\frac{\tilde{S}(E')}{E'-E}dE' , \tag{3.17}$$

where $\tilde{R}(E)$ and $\tilde{s}(E)$ are quadratic functions, see Eqs. (3.15) and (3.16). In Fig. 5 the short-dashed curve shows $\tilde{R}(E)$ and the long-short-dashed curve shows $R_1^{\text{ext}}(E)$. Both have been reproduced from Fig. 3(c). If this external R function is exact for the domain D_1, then for the smaller domain $D_2=(E_l,E_{u2})$ with $E_{u2}=0.5$ MeV, the scattering function is given *exactly* by the expression (3.1), with

$$R(E)=R_2^{\text{ext}}(E)+\sum_{\lambda=1}^{10}\frac{\gamma_\lambda^2}{E_\lambda-E} , \tag{3.18}$$

where now

$$R_2^{\text{ext}}(E)=R_1^{\text{ext}}(E)+\sum_{\Lambda=11}^{20}\frac{\gamma_\Lambda^2}{E_\Lambda-E} . \tag{3.19}$$

These values of $R_2^{\text{ext}}(E)$ are represented by the solid curve in Fig. 5.

If the replacement of the sum over Λ on the right-hand side of Eq. (3.19) by an integral is accurate, the values of $R_2^{\text{ext}}(E)$ should be approximated by

$$R_2^{\text{ext}}(E)\simeq\tilde{R}(E)-\mathrm{P}\int_{E_l}^{E_{u2}}\frac{\tilde{s}(E')}{E'-E}dE' . \tag{3.20}$$

The latter quantity is represented by the long-dashed curve in Fig. 5. The close agreement of the long-dashed and solid curves establishes the accuracy of our treatment of the poles lying outside the experimental domain. It also implies that Eq. (3.4) yields an average scattering function which is independent of the size of the experimental domain, provided the domain contains enough resonances to enable one to determine the strength function $\tilde{s}(E)$ with sufficient accuracy.

IV. FLUCTUATION CONTRIBUTIONS

The picket-fence models are idealizations of the physical reality. In practice the existence of statistical fluctuations of the resonance parameters does not always enable one to obtain a very accurate value of $\tilde{s}(E)$ in the experimental domain. We now describe how the effect of the fluctuations of $\langle\gamma_\lambda^2\rangle/d$ about its average $\tilde{s}(E)$ can be taken into account in the algebraic prescription for calculating the average scattering function.

The contribution to the quantity $R(E+iI)$ of the resonances contained in the experimental domain D can be explicitly taken into account by rewriting Eq. (2.6) as

$$R(E+iI)=\sum_{E_\lambda\in D}\frac{\gamma_\lambda^2}{E_\lambda-E-iI}-\int_{E_l}^{E_u}\frac{\tilde{s}(E')}{E'-E-iI}dE' + \int_{-\infty}^{\infty}\frac{s(E')}{E'-E-iI}dE' , \tag{4.1}$$

where $s(E)$ is a smooth function which is approximated by $\tilde{s}(E)$ within D. Under condition (2.4), the last term on the right-hand side of this equation is approximately equal to

$$\mathrm{P}\int_{-\infty}^{\infty}\frac{s(E')}{E'-E}dE'+i\pi\tilde{s}(E)\ . \tag{4.2}$$

The first two terms on the right-hand side of Eq. (4.1) account for possible deviations of $\langle\gamma_\lambda^2\rangle/d$ from the smooth value assumed for $\tilde{s}(E)$.

Equation (4.1) leads to the following modification of the prescription (3.4):

$$\langle S(E)\rangle_I=\frac{1+i\{[\tilde{R}(E)+R^f(E)]+i\pi[\tilde{s}(E)+s^f(E)]\}}{1-i\{[\tilde{R}(E)+R^f(E)]+i\pi[\tilde{s}(E)+s^f(E)]\}}\ , \tag{4.3}$$

where

$$s^f(E)=\frac{I}{\pi}\sum_{\lambda=1}^{N}\frac{\gamma_\lambda^2}{(E_\lambda-E)^2+I^2}-\frac{I}{\pi}\int_{E_l}^{E_u}\frac{s(E')}{(E'-E)^2+I^2}dE' \tag{4.4}$$

and

$$R^f(E)=\sum_{\lambda=1}^{N}\frac{\gamma_\lambda^2(E_\lambda-E)}{(E_\lambda-E)^2+I^2}-\int_{E_l}^{E_u}\frac{s(E')(E'-E)}{(E'-E)^2+I^2}dE'\ . \tag{4.5}$$

In the picket fence models considered in the preceding section, the fluctuation corrections (4.4) and (4.5) are negligible because we used the exact $\tilde{s}(E)$ in the calculation of the right-hand side of Eq. (3.4). To demonstrate the effects of fluctuations, we now consider an example where the E_λ, $\tilde{s}$, $\tilde{R}(E)$, and $R^{\mathrm{ext}}(E)$ are each the same as in Fig. 1 but where the uniform picket fence is replaced by the fluctuating structure of Fig. 6(a). These reduced widths were selected at random from a Porter-Thomas[16] distribution with the constraint that the sum of reduced widths in the domain be the same as for the picket fence of Fig. 1(a). The short-dashed curves in Figs. 6(b) and (c) show the $\tilde{s}$ and $\tilde{R}(E)$ reproduced from Fig. 1.

Using this example we averaged with $I=100$ keV both numerically and by the algebraic prescription Eq. (4.3). The solid curves in Fig. 6 show the numerical average in terms of $\bar{R}(\bar{E})$ and $\bar{s}(\bar{E})$ and the long dashed curves show $[\tilde{R}(E)+R^f(E)]$ and $[\tilde{s}(E)+s^f(E)]$. The good agreement between the two sets of curves confirms that the prescription (4.3) is a good approximation to the numerical average.

The use of expression (4.3) with the fluctuating terms included allows one to study nonstatistical effects (e.g., intermediate structure). However, actual physical scattering functions are often similar to the present example for which the fluctuations are merely statistical. In that case it is useful to average over the fluctuations in order to produce a smooth function for comparison to an optical model scattering function. This is accomplished in (4.3) by making I very large so that the fluctuating terms are negligible. Thereby, expression (4.3) is reduced to (3.4) to give the same smooth average for this example as for the original picket fence of Figs. 1 and 2. Alternatively, we can describe the smoothing process by two steps in which we first replace the fluctuating structure by a picket fence

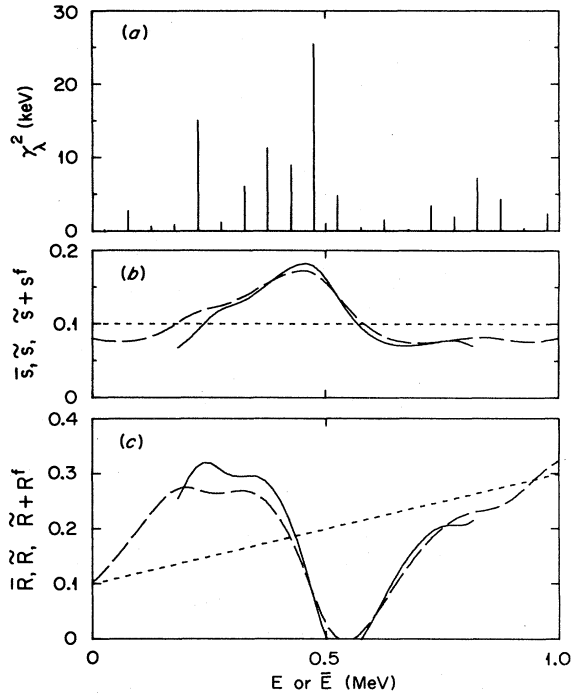

FIG. 6. Effects of fluctuations: (a) shows reduced widths for equally spaced levels. (b) and (c) show (short dash) $\tilde{R}(E)$ and $\tilde{s}(E)$ from Fig. 1, (solid) $\bar{R}(\bar{E})$ and $\bar{s}(\bar{E})$ from the numerical average for Lorentzian weighting with $I=100$ keV, and (long dash) $[\tilde{R}(E)+R^f(E)]$ and $[\tilde{s}(E)+s^f(E)]$ from prescription (4.3).

with the same average strength function and we then average with a small $I\simeq d$. For the latter description the averaging process with small I is consistent with the discussion in Sec. II.

The statistical fluctuations for an actual nucleus usually make it difficult to detect an energy dependence in $\tilde{s}(E)$ similar to our second example of Figs. 3–5. The inclusion of the fluctuating terms might help to show a dependence; however, it is important also to include the information available from the quantity $R^{\mathrm{ext}}(E)$, which is less influenced by statistical effects. In our example of the rising picket fence the $R^{\mathrm{ext}}(E)$ of Fig. 3(c) could have been described with the assumption that $\tilde{s}$ in Eq. (2.16) is a constant equal to 0.095, as deduced from the sum of γ_λ^2, but the corresponding $\tilde{R}(E)$ would have a relatively strong energy dependence. Such a strong dependence would be inconsistent with an optical model interpretation.

V. OPTICAL MODEL SCATTERING FUNCTION

The general form of the N level plus background R-matrix parametrization of the elastic part of the scattering function reads

$$S_p^{lj}(E)=e^{2i\phi_l(E)}\frac{1-L_l^*(E)R_{lj}(E)}{1-L_l(E)R_{lj}(E)}\ , \tag{5.1}$$

with

$$R_{lj}(E)=R_{lj}^{\rm ext}(E)+\sum_{\lambda=1}^{N}\frac{\gamma_\lambda^2}{E_\lambda-E}\ . \tag{5.2}$$

Here, $\phi_l(E)$ is the hard sphere scattering phase shift, while

$$L_l(E)=S_l(E)-B_l+iP_l(E)\ , \tag{5.3}$$

where $S_l(E)$ is the shift function, B_l the boundary parameter, and $P_l(E)$ the penetration factor.

The reasoning carried out in Sec. II and the examples considered in Sec. III lead one to define in the (l,j) subspace the spherical optical-model potential $\mathscr{V}_{\rm OM}^{lj}(r;E)$ by the following requirement. For E contained inside the experimental domain $D=(E_l,E_u)$, $\mathscr{V}_{\rm OM}^{lj}(r;E)$ must be determined in such a way that the asymptotic value for large r of the optical-model wave function $\psi_{\rm OM}(\mathbf{r};E)$ defined by the wave equation

$$\left[-\frac{h^2}{2m}\nabla^2+\mathscr{V}_{\rm OM}(\mathbf{r};E)\right]\psi_{\rm OM}(\mathbf{r};E)=E\psi_{\rm OM}(\mathbf{r};E) \tag{5.4}$$

yields the following value for the optical-model scattering function:

$$S_{\rm OM}^{lj}(E)=e^{2i\phi_l(E)}\frac{1-L_l^*(E)R_{lj}^{\rm OM}(E)}{1-L_l(E)R_{lj}^{\rm OM}(E)}\ , \tag{5.5}$$

where

$$R_{lj}^{\rm OM}(E)=\tilde{R}_{lj}(E)+i\pi\tilde{s}_{lj}(E)\ , \tag{5.6}$$

with

$$\tilde{R}_{lj}(E)=R_{lj}^{\rm ext}(E)+\int_{E_l}^{E_u}\frac{\tilde{s}_{lj}(E')}{E'-E}dE'\ ; \tag{5.7}$$

$\tilde{s}_{lj}(E)$ is the observed strength function for $E\in D$. We note that the variable E at which the quantities $\phi_l(E)$ and $L_l(E)$ on the right-hand side of Eq. (5.5) are evaluated is the same energy at which Eq. (5.4) is solved. This corresponds to the fact that in Sec. II the quantities $\phi_0(E)$ and $P_0(E)$ have not been averaged over. Physically this reflects the property that the penetration factor and related quantities are automatically evaluated at the energy E when solving Eq. (5.4). Our summary in Sec. VII includes a comment on the parametrization of the optical model.

VI. INSENSITIVITY TO THE BOUNDARY CONDITIONS

From the preceding section we conclude that the numerical average of the general scattering function (5.1) should be performed for the assumed boundary conditions with the quantities $\phi_l(E)$ and $L_l(E)$ fixed at the average energy $\bar{E}$. Actually, for our examples in Sec. III we chose the constants $\phi_l=0$, $P_l=1$, and $S_l-B_l=0$. That was permissible because we then used the *same* constants in Eq. (3.11) to express the averages in terms of the quantities, $\bar{R}(\bar{E})$ and $\bar{s}(\bar{E})$. In the more general case we average the function (5.1) with the constants as stated in the preceding section and then express the average using the *same* constants:

$$\bar{S}_p^{lj}(\bar{E})=e^{2i\phi_l(\bar{E})}\frac{1-L_l^*(E)[\bar{R}_{lj}(\bar{E})+i\pi\bar{s}_{lj}(\bar{E})]}{1-L_l(\bar{E})[\bar{R}_{lj}(\bar{E})+i\pi\bar{s}_{lj}(\bar{E})]}\ . \tag{6.1}$$

We expect $\bar{R}_{lj}(\bar{E})$ and $\bar{s}_{lj}(\bar{E})$ for a *given* R function to be insensitive to the particular partial wave or boundary conditions.

To demonstrate this insensitivity we repeated the numerical averages of the models of Sec. III using various assumed partial waves and boundary conditions (i.e., $l=0$, 1, and 2; $a=5.5$ and 8 fm; $B_l=S_l$ and $-l$). In each case we used the constants $\phi_l(\bar{E})$, $P_l(\bar{E})$, and $S_l(\bar{E})$ not only in Eq. (5.1) for averaging but also in Eq. (6.1) for expressing the averages in terms of a complex R function. The resulting $\bar{R}_{lj}(\bar{E})$ and $\bar{s}_{lj}(\bar{E})$ showed only slight variations from the curves already plotted in Sec. III. For example, in Fig. 7 the solid curves show $\bar{R}(\bar{E})$ and $\bar{s}(\bar{E})$ reproduced from Fig. 6 and the dashed curves show these quantities calculated for $l=2$ with the boundary conditions $a=8$ fm and $B_l=S_l$. The two sets of curves are nearly identical.

On the other hand, in order to compare the numerical average of $S_p^{lj}(E)$ to the function $S_{\rm OM}^{lj}(E)$ of Eq. (5.4), we must use the same boundary conditions as used for the original R-function expansion (5.1). We expect these average scattering functions, and consequently $\mathscr{V}_{\rm OM}^{lj}(r;E)$, to be approximately independent of the choice of the boundary conditions. This independence has been discussed in Ref. 17.

In order to present an example of this independence, we actually chose the two R functions of Figs. 1 and 3 such that they give the same s-wave scattering function for two different boundary radii, i.e., $a=5.5$ fm for the uniform picket fence of Fig. 1 and $a=8$ fm for the rising picket fence in Fig. 3. (For both cases $B_0=0$.) The 5.5-fm radius corresponds to 1.4 $A^{1/3}$ for $A=60$ and the 8-fm radius to the distance at which a typical real Woods-Saxon potential has fallen to about 1% of its central value. To illustrate that the scattering function $S(E)$ is the same for the

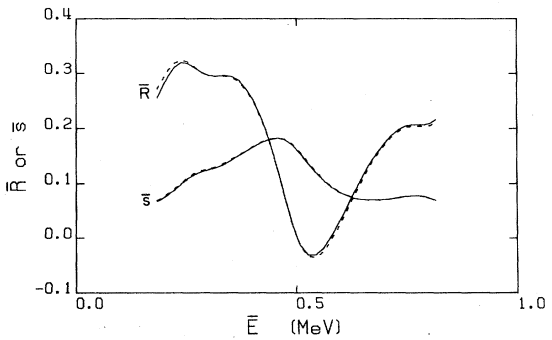

FIG. 7. An example for a given R function of the insensitivity of $\bar{R}$ and $\bar{s}$ to the particular partial wave and boundary conditions. The solid curves are reproduced from Fig. 6 and the dashed curves are for $l=2$, $a=8$ fm, and $B_l=S_l$.

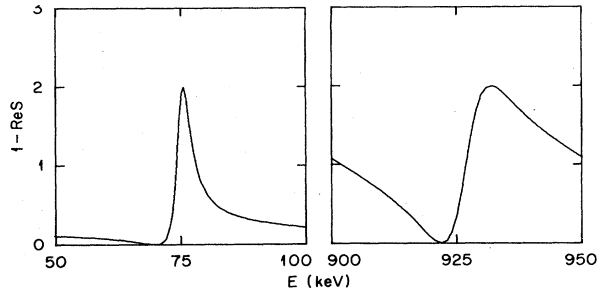

FIG. 8. Examples of s-wave resonances for the uniform model (see Fig. 1) with a 5.5-fm boundary radius and for the rising picket fence model (see Fig. 3) with an 8-fm radius. Both models give the same curves.

two boundary radii we show in Fig. 8 the quantity $[1-ReS(E)]$ for both radii for the 75- and 925-keV resonances. The curves for the two radii and corresponding R functions are identical.

Using Lorentzian weighting with $I=100$ keV we have averaged these two equivalent scattering functions with $\phi_0(E)$ and $P_0(E)$ fixed at $\overline{E}$, as stated above. To present these results we plot the compound and shape elastic cross sections:

$$\sigma_c(\overline{E})=\pi k^{-2}g[1-|\overline{S}(\overline{E})|^2] \tag{6.2}$$

and

$$\sigma_{se}(\overline{E})=\pi k^{-2}g\,|1-\overline{S}(\overline{E})|^2\,, \tag{6.3}$$

where g is the spin statistical factor. In Fig. 9 the solid curves show these quantities plotted for the two R functions and corresponding radii. There are negligible differences between the two.

For the corresponding algebraic prescription we have

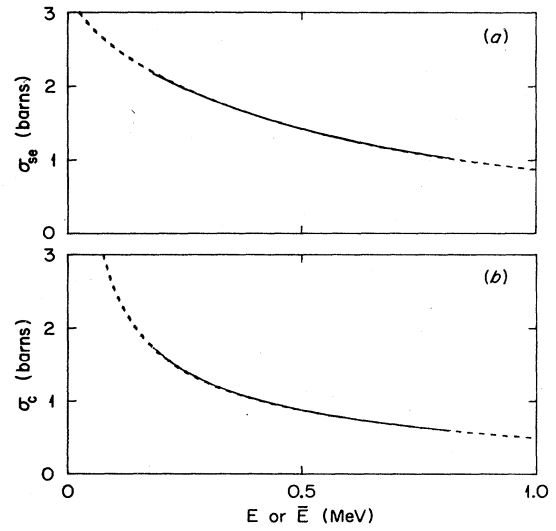

FIG. 9. Compound and shape elastic cross sections for the s-wave model for either Fig. 1 with a 5.5-fm radius or Fig. 3 with an 8-fm radius. Solid curves show $\sigma_{se}(\overline{E})$ and $\sigma_c(\overline{E})$ for $I=100$ keV. Dashed curves show $\sigma_{se}(E)$ and $\sigma_c(E)$ calculated from $\tilde{R}(E)$ and $\tilde{s}(E)$. In each case, dashed or solid, the curves for the two radii are nearly identical.

$$\langle S(E)\rangle=e^{2i\phi_0(E)}\frac{1+iP_0(E)[\tilde{R}(E)+i\pi\tilde{s}(E)]}{1-iP_0(E)[\tilde{R}(E)+i\pi\tilde{s}(E)]}\,, \tag{6.4}$$

where ϕ_0 and P_0 are evaluated at the assumed radii for the respective $\tilde{R}(E)$ and $\tilde{s}(E)$. In Fig. 9 the dashed curves show the resulting $\sigma_{se}(E)$ and $\sigma_c(E)$ which have been calculated by analogy with Eqs. (6.2) and (6.3) with $\overline{S}(\overline{E})$ replaced by $\langle S(E)\rangle$. Again the differences for the two radii are negligible. Also, as expected, the numerical average and algebraic prescription are in good agreement for $\overline{E}=E$.

VII. SUMMARY

At low neutron energies of less than a few MeV a scattering function which has been deduced by an R-matrix analysis of experimental cross sections can easily be energy averaged for each individual partial wave in order to compare to an optical model scattering function, provided the external R function is parametrized as in Eq. (2.16). In that equation $\tilde{s}(E)$ is the observed strength function, $\langle\gamma_\lambda^2\rangle/d$, and $\tilde{R}(E)$ is a simple parametric function. Given this parametrization the comparison to the optical model is made simply by Eq. (5.5). The analysis is insensitive to the assumed boundary conditions provided that these conditions are used consistently. In general the strength function $\tilde{s}(E)$ varies slowly with energy. Expressing the external R function as in Eq. (2.16) can help to reveal this energy dependence, which may otherwise be obscured by the statistical fluctuations in γ_λ^2. An experiment which shows clear evidence for intermediate structure might require the addition of fluctuating terms to $\tilde{R}(E)$ and $\tilde{s}(E)$ [see Eqs. (3.25)—(3.27)]. Such effects would require explicit treatment beyond the scope of the spherical optical model.

The description of the averaged scattering function with a phenomenological optical model potential requires the adjustment of model parameters. However, the fact that the scattering function is to be fit for individual partial waves requires a different procedure than is usually used at higher energies. To achieve a fit for a given partial wave one can usually[4,15] adjust one parameter for the real potential and another for the imaginary potential. Thus one may find an l-dependent or parity-dependent model which should then be compared to models deduced at other energies.

ACKNOWLEDGMENTS

We are grateful to Dr. J. A. Harvey, Dr. D. J. Horen, Dr. N. M. Larson, Dr. J. E. Lynn, and Dr. H. A. Weidenmüller for helpful discussions. We are also indebted to Dr. A. D. MacKellar for a careful reading of this manuscript. C. Mahaux thanks the Oak Ridge National Laboratory for sponsoring the visit to Oak Ridge which made this collaboration possible. This research was sponsored by the Division of Nuclear Sciences, U. S. Department of Energy, under Contract Nos. DE-AC05-840R21400 with Martin Marietta Energy Systems, Inc. and DE-AC02-76-ER02696 with Denison University.

[1]A. M. Lane and R. G. Thomas, Rev. Mod. Phys. **30**, 257 (1958).
[2]G. E. Brown, Rev. Mod. Phys. **31**, 893 (1959).
[3]J. E. Lynn, *The Theory of Neutron Resonance Reactions* (Clarendon, Oxford, 1968).
[4]C. H. Johnson and R. R. Winters, Phys. Rev. C **21**, 2190 (1980).
[5]C. H. Johnson and R. R. Winters, Phys. Rev. C **27**, 416 (1983).
[6]C. H. Johnson, N. M. Larson, C. Mahaux, and R. R. Winters, Phys. Rev. C **27**, 1913 (1983).
[7]W. M. MacDonald, Nucl. Phys. **A395**, 221 (1983).
[8]W. M. MacDonald and M. C. Birse, Nucl. Phys. **A403**, 99 (1983).
[9]A. D. MacKellar and B. Castel, Phys. Rev. C **28**, 441 (1983).
[10]W. M. MacDonald and M. C. Birse, Phys. Rev. C **29**, 1560 (1984).
[11]C. H. Johnson, N. M. Larson, C. Mahaux, and R. R. Winters, Phys. Rev. C **29**, 1563 (1984).
[12]R. F. Carlton, J. A. Harvey, and C. H. Johnson, C **29**, 1988 (1984).
[13]A. D. MacKellar and B. Castel, Phys. Rev. C **29**, 1993 (1984).
[14]C. H. Johnson, in *Neutron-Nucleus Collisions—A Probe of Nuclear Structure—1984 (Glouster, Ohio),* Proceedings of the Conference on Neutron-Nucleus Collisions—A Probe of Nuclear Structure, AIP Conf. Proc. No. 124, edited by J. Rapaport, R. W. Finlay, S. M. Grimes, and F. S. Dietrich (AIP, New York, 1985), p. 446.
[15]R. R. Winters, C. H. Johnson, and A. D. MacKellar, Phys. Rev. C **31**, 384 (1985).
[16]C. E. Porter and R. G. Thomas, Phys. Rev. **104**, 483 (1956).
[17]J. Cugnon and C. Mahaux, Phys. Rev. C **10**, 4 (1974).